Injection Length in Staggered Organic Thin Film Transistors: Assessment and Implications for Device Downscaling

Dario Natali, Jiaren Chen, Francesco Maddalena, Francisco García Ferré, Fabio Di Fonzo, and Mario Caironi*

In staggered thin film transistors, the injection length is the fraction of the gate to contact overlap that is effectively involved in current injection. Its assessment is important to properly downscale device dimensions. In fact, in order to increase transistor operation speed, the whole device footprint should be downscaled, which means both the gate to contact overlap and the channel length, as they affect the relative weight of gate to contact parasitic capacitances and the carrier transit time along the channel respectively. Nevertheless, it is not advisable to make the gate to contact overlap smaller than the injection length, because this negatively affects contact resistances. Suitable figures of merits are introduced to quantify these aspects, and a method is proposed to extract the injection length from electrical measurements. As an example of application, transistors based on the prototypical n-type polymer poly{[*N*,*N*′-bis(2-octyldodecyl)-naphthalene-1,4,5,8-bis(dicarboximide)-2,6-diyl]-alt-5,5′-(2,2′-bithiophene)} (P(NDI2OD-T2) are analyzed. When the channel length is scaled while driving voltages are kept constant, in P(NDI2OD-T2) the injection length decreases as well, thus proving that the downscaling of the whole device footprint is feasible. The physical origins of this finding are analyzed and traced back to material properties, in order to suggest general guidelines for a successful transistor downscaling.

1. Introduction

Organic semiconductors have attracted large attention for electronics applications due to their advantages in terms of mechanical flexibility, light weight, and possibility of covering large-area with low fabrication cost.[1] An increasing number of organic semiconductors show carrier mobility in excess of 5 $cm^2\ V^{-1}\ s^{-1}$ when employed as active materials in long (>10 µm) channel organic thin film transistors (OTFT).[2–12] Therefore by scaling the channel length down to 10–1 µm, in principle OTFTs should be able to operate at relatively high (1–10 MHz) frequencies at reasonable (<10 V) applied voltages.[13] In practice, apart from some reports,[13–22] this is often not easy to achieve because of injection issues:[23,24] contact resistances tend to become dominant over the channel resistance in short channel transistors reducing the expected improvement of device performances.[25] This situation is severely limiting the range of applications for OTFTs.[26] Indeed contact resistances arise from contact/semiconductor interface properties hence they are not expected to scale with the transistor channel length. To address this issue not only suitable modifications of the contact/semiconductor interface aimed at enhancing the contact injecting properties have to be implemented,[27] but also the device topology has to be considered. Staggered OTFTs, where the contacts and the transistor channel do not lie in the same plane, are usually characterized by lower contact resistances than coplanar ones:[28] while in these latter the injection area is limited by the accumulated channel depth (few nanometers), in the former the overlap between gate and source/drain contacts (many micrometers or even tens of micrometers) can be exploited, as shown in **Figure 1**. The gate/contact overlapping length has to be suitably engineered: on the one hand it should be large enough to accommodate the injected current and to minimize contact resistances; but on the other hand it should not be too large because overlapping areas not effectively involved in injection solely result in additional parasitic capacitances that deteriorate the device speed.[13,29] It is therefore important to quantify the injection length, which is the length over which sizeable carrier injection occurs.[30,31]

Despite the large number of studies on contact effects in OTFTs,[24,32] few of them discuss the effect of the gate to contact overlap: Xu et al. found a relationship between the optimal contact length and the semiconductor thickness in staggered OTFT.[33] Park et al. found that threshold voltage, field effect mobility and contact resistances are affected by the contact length in staggered OTFT;[34] Wang et al. simulated the effect of contact length scaling.[35] Ante et al. studied the effect of contact

Prof. D. Natali, J. Chen, Dr. F. Maddalena, Dr. F. García Ferré, Dr. F. Di Fonzo, Dr. M. Caironi
Center for Nano Science and Technology @PoliMi
Istituto Italiano di Tecnologia
Via Pascoli 70/3, 20133 Milano, Italy
E-mail: dario.natali@polimi.it
Prof. D. Natali
Dipartimento di Elettronica
Informazione e Bioingegneria
Politecnico di Milano
P.za L. da Vinci, 32, 20133 Milano, Italy

DOI: 10.1002/aelm.201600097

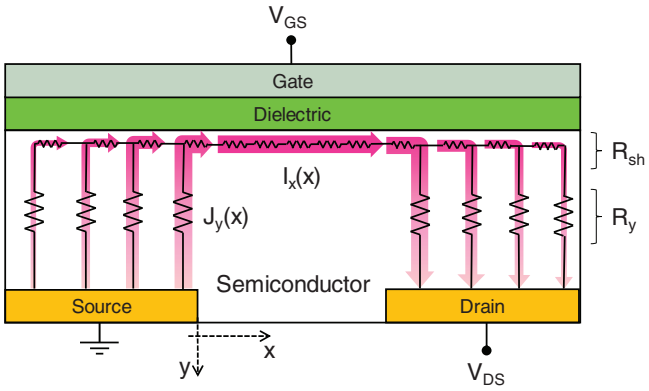

Figure 1. Sketch of the cross-section of a top-gate bottom-contact transistor affected by current crowding effect. $J_y(x)$ flows parallel to the *y*-axis in the gate–contacts overlap region, and is crowded close to the source/drain gap; in the source/drain gap region, the current $I_x(x)$ flows along the *x*-axis only. Adapted with permission.[12]

length relying upon the transfer line method (TLM),[13] whose applicability has been recently shown to be questionable in staggered OTFTs affected by non-quasi-ohmic injection.[36]

In this work we propose an easy and general method for the assessment of the injection length in staggered OTFTs and we apply it to poly{[*N*,*N*′-bis(2-octyldodecyl)-naphthalene-1,4,5,8-bis(dicarboximide)-2,6-diyl]-alt-5,5′-(2,2′-bithiophene)} (P(NDI2OD-T2)), a printable, prototypical n-type polymer with a high mobility, exceeding 1 $cm^2\ V^{-1}\ s^{-1}$ when processed from suitable pre-aggregating solvents.[11,37] Interestingly enough we find that in P(NDI2OD-T2) the injection length scales with the channel length when applied voltages are kept constant, resulting in a much more favorable downscaling than expected. Our methodology allows to rationalize and to generalize this result, which is valid for all staggered transistors where the electrode-semiconductor injection process is dominating over the semiconductor bulk contribution.[38] This finding provides a clear guideline for the development of high performance and downscaled OTFTs, underlining the importance of developing π-conjugated materials with enhanced bulk transport properties.

2. Current Crowding Modeling and Design Rules

Injection in staggered OTFTs is often discussed in the framework of the current crowding effect.[24,31] Here we provide a brief introduction taking top-gate bottom-contact (TGBC) n-type OTFT as reference and introduce some basic design rules. We assume that the device is biased in the linear regime. When the OTFT is on (i.e. when the gate voltage V_G is higher than the threshold voltage V_T), in static conditions the accumulation layer is induced over the whole semiconductor area below the gate electrode, comprising the gate–contacts overlapping regions as well, whose length we call L_{OV} (**Figure 2**). With reference to the scheme in Figure 1, the injected current flows parallel to the *y*-axis from the source contact into the accumulated channel located in the overlap region, and then proceeds along the accumulated channel parallel to the *x*-axis.

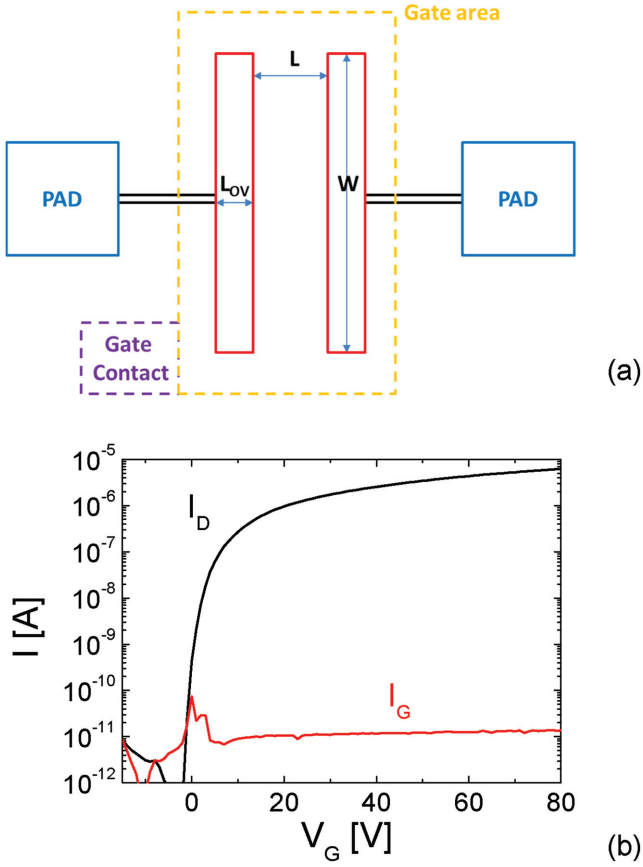

Figure 2. a) Layout of the transistor: L_{OV}, *L*, and *W* denote gate–electrode overlap length, channel length, and electrode width, respectively. Contact pads (in blue), electrodes (in red), and connecting paths between pads and electrodes (in black) are the bottom contact pattern; the gate area (in yellow) and gate contact pad (in violet) represent the pattern in the topmost layer. Semiconductor and dielectric layers are not drawn in the figure. b) Transfer characteristic curves of TFTs with L_{OV} = 5 μm W = 1 mm, L = 40 μm measured at V_{DS} = 8 V.

We term $J_y(x)$ the current density flowing in *y* direction across the bulk of the semiconductor; we model $J_y(x) = V(x)/R_y$, where R_y is a resistance per unit area taking into account injection and transport across the bulk, viz. $R_y = R_{contact} + R_{bulk}$, and $V(x)$ is the electrical potential at the semiconductor/insulator interface. $I_x(x)$ is the current flowing in *x* direction along the accumulated channel, this latter being characterized by a sheet resistance $R_{sh} = [\mu C_{ins}(V_{GS} - V_T)]^{-1}$, where μ is the carrier mobility and C_{ins} is the dielectric capacitance per unit area. We now focus on the region where contacts and gate overlap, viz. $-L_{OV} < x < 0$. A detailed analytical modeling[39] shows that the source/drain contact resistance R_C can be expressed as[30]

$$R_C = \frac{R_y}{WL_0 \tanh\left(L_{OV}/L_0\right)}, \quad (1)$$

where L_0, termed injection length, is equal to $\sqrt{R_y/R_{sh}}$. R_C is a decreasing function of L_{OV}/L_0 (see also Figure S1a in the Supporting Information). To elucidate the physics behind, we consider two limiting cases.

If $L_{OV} \gg L_0$, the hyperbolic function in Equation (1) tends to 1 and the contact resistance approaches its minimum asymptotical value $R_{CMIN} = R_y/WL_0$: L_{OV} is large enough not to hamper carrier injection and as a matter of fact it does not enter into the expression of R_{CMIN}. It can be shown that the x-dependence of J_y, I_x, and V_x is given by an increasing exponential with a characteristic length L_0, and that the injection current is crowded close to $x = 0$ (Figure S1b, Supporting Information). The parameter L_0 thus measures the crowding degree, as the region comprised between $-L_0$ and 0 accommodates 63% of the whole injected current.

If on the contrary $L_{OV} \ll L_0$, first-order approximation of $\tanh(L_{OV}/L_0) \approx L_{OV}/L_0$ yields $R_C = R_y/WL_{OV}$: L_{OV} is actually limiting charge injection and the whole L_{OV} is exploited to accommodate the injection current.

As a rule of thumb, we observe that for $L_{OV}/L_0 = 0.5$, 1, 1.5 then R_C is 116%, 30%, 10% larger than its asymptotic minimum value R_{CMIN} (Figure S1a, Supporting Information).

2.1. Design Rules

In view of device downscaling, it is more useful to compare the contact resistance to the channel resistance rather than focusing on the contact resistance absolute value.

To this extent we introduce as figure of merit the relative weight of contact resistances with respect to overall device resistance, viz. $R_{CREL} = R_{CTOT}/(R_{CTOT} + R_{CH})$, where R_{CTOT} is the sum of source (R_S) and drain (R_D) contact resistances. Assuming that $R_S = R_D$ it can be shown that

$$R_{CREL} = \frac{1}{1 + \frac{1}{2}\frac{L}{L_0}\tanh\left(\frac{L_{OV}}{L_0}\right)} \quad (2)$$

Equation (2) shows that R_{CREL} only depends on three lengths: two of them, L and L_{OV}, are geometrical parameters, whereas material properties and gate biasing define L_0. A 2D color map of R_{CREL} as a function of L/L_0 and L_{OV}/L_0 is reported in **Figure 3**. It is instructive to note that already for $L_{OV}/L_0 = 1.5$ ($L_{OV}/L_0 = 3$) the hyperbolic tangent term is equal to 0.9 (0.99); thus as a rule of thumb, once that $L_{OV}/L_0 \geq 1.5$ L_{OV}, R_{CREL} gets dominated by the ratio L/L_0. In this regime, further increasing L_{OV} has little or no effect on R_{CREL}, whereas scaling the channel length below L_0 is not advisable as it would result in severe contact limitation: indeed already for $L = L_0$ contact resistances are just as large as the channel resistance.

In the following, quantitative design rules to achieve a target R_{CREL} are derived. It is relatively difficult to act on L_0, since it depends on material parameters and on the square root of the gate bias. Therefore we assume that L_0 is fixed and we consider L and L_{OV} the degrees of freedom that can be exploited. Equation (2) can be rewritten in order to highlight the relation between L and L_{OV}, viz. $\frac{2(R_{CREL}^{-1} - 1)}{L/L_0} = \tanh(L_{OV}/L_0)$. This latter expression can be actually regarded as a design rule: for a given L_0, in order to obtain the desired value for R_{CREL}, L and L_{OV} cannot be chosen independently but must fulfil this relation. Furthermore, since $\tanh(L_{OV}/L_0) \leq 1$, the ratio L/L_0 is lower bounded: $L/L_0 > 2(R_{CREL}^{-1} - 1)$. Quantitatively speaking, if the target is $R_{CREL} = 10\%$ ($R_{CREL} = 20\%$), then the minimum value for L/L_0 is 18 (8). If L/L_0 is larger than this minimum, L_{OV}/L_0 can be made accordingly smaller. Another possible scenario is the one where not only a certain value for R_{CREL} has to be guaranteed but, as an additional constraint, the device footprint, viz. $L + L_{OV}$, has to be minimized. In this case it can be shown that optimum values are given by $L/L_0 = \sqrt{4(R_{CREL}^{-1})^2 - 6R_{CREL}^{-1} + 2}$ and $L_{OV}/L_0 = \tanh^{-1}\sqrt{\frac{2(R_{CREL}^{-1} - 1)}{2(R_{CREL}^{-1} - 1)}}$. If $R_{CREL} = 10\%$ ($R_{CREL} = 20\%$), then the optimum values are as follows: L/L_0 is about 18.5 (8.5), L_{OV}/L_0 about 2.15 (1.76) and the total minimized device length $(L + L_{OV})/L_0$ about 20.65 (10.24).

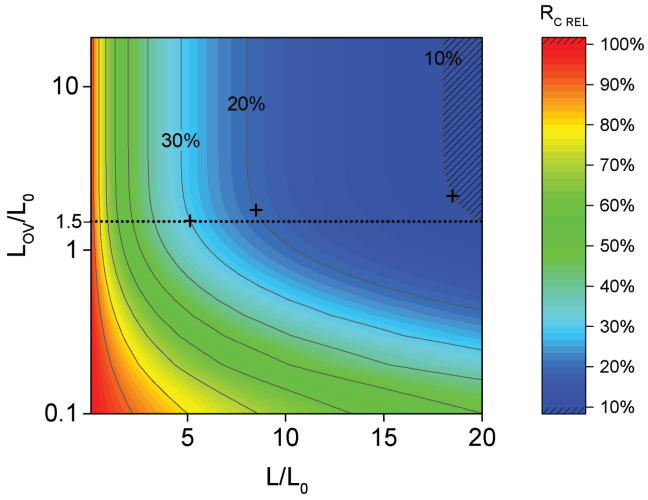

Figure 3. R_{CREL} as function of L/L_0 and L_{OV}/L_0. Contour lines for R_{CREL} = 10%, 20%, and 30% are reported; crosses represent, for a given R_{CREL}, the combination of L/L_0 and L_{OV}/L_0 minimizing the device footprint. For $L_{OV}/L_0 \geq 1.5$, R_{CREL} is practically set by the ratio L/L_0 only ($L_{OV}/L_0 = 1.5$ is highlighted by the dashed line).

From this discussion it is clear that L_0 is a key quantity and that its assessment is mandatory for a proper device design.

2.2. Simplified Models

In order to avoid the complexity of the hyperbolic function in the extraction of device parameters from experimental measurements, we introduce suitable approximations for Equation (1) depending on the relative magnitude of L_0 with respect to L_{OV}. In the following a gate-voltage-dependent mobility $\mu = \mu_0 (V_G - V_T)^\gamma$ is assumed according to the model developed by Vissenberg and Matters.[40] The sheet resistance thus becomes $R_{sh} = [\mu_0 C_{ins}(V_{GS} - V_T)^{(\gamma+1)}]^{-1}$. We limit our analyses to the linear regime of operation for the OTFT.

2.2.1. Case $L_{OV} < L_0$

We expand Equation (1) to third order assuming $L_{OV} < L_0$ and after some arrangements we have

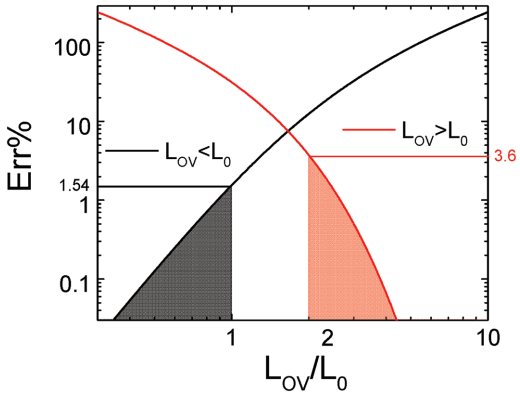

Figure 4. Percent error as a function of L_{OV}/L_0 introduced by the approximated contact resistances: Equation (3) ($L_{OV} < L_0$, black curve); Equation (5) ($L_{OV} > L_0$, red curve). Shaded areas represent the region where the percent error introduced by Equation (3) (Equation (5)) is below 1.54% (3.6%).

$$R_C = \frac{R_\gamma}{WL_{OV}} + \frac{1}{3}\frac{L_{OV}}{W} R_{sh} = R_{C_\gamma} + R_{C_x}(V_G), \quad (3)$$

R_C in Equation (3) is the sum of a constant term related to carrier flow in y-direction, denominated R_{C_γ}, and of a gate-voltage-dependent term related to carrier flow in x-direction denominated $R_{C_x}(V_G)$. The former term can be understood as the injection and bulk resistance assuming that the injection area is WL_{OV}, whereas in the latter term the multiplying factor 1/3 takes into account the non-uniform distribution of $I_x(x)$. As shown in **Figure 4**, the approximate expression of Equation (3) has a good degree of accuracy already starting from $L_{OV} = L_0$, where the relative error is as low as 1.54%; hence it is sufficient that $L_{OV} \leq L_0$ for this simplification to hold.

We have now to consider that what we extract from experimental measurements (see Section 3.) is R_{CTOT}, viz. the sum of source and drain contact resistances q. 4:

$$R_{C\,TOT} = R_S + R_D = \frac{R_{\gamma,S} + R_{\gamma,D}}{WL_{OV}} + \frac{2}{3}\frac{L_{OV}}{W}\frac{1}{\mu_0 C_{ox}(V_G - V_T)^{\gamma+1}} = R_{C\,TOT_\gamma} + R_{C\,TOT_x}(V_G). \quad (4)$$

Equation (4) takes into account that R_{C_γ} can be different at source and drain, since the metal/semiconductor Schottky junction is forward biased at the former but reverse biased at the latter. On the contrary $R_{C_x}(V_G)$ is the same at source and drain.

2.2.2. Case $L_{OV} > L_0$

For $L_{OV} > L_0$, the hyperbolic function in Equation (1) can be approximated to 1 and the total contact resistance can be written as

$$R_{C\,TOT} = \frac{R_{\gamma,S} + R_{\gamma,D}}{WL_0} = \frac{R_{\gamma\,TOT}}{WL_0}. \quad (5)$$

Equation (5) shows that R_{CTOT} can be thought as due to injection and transport along y-axis across a V_G-dependent area given by WL_0. R_{CTOT} depends on the square root of the sheet resistance, viz. $R_{C\,TOT} \propto \sqrt{R_{sh}} \propto (V_G - V_T)^{-(\gamma+1)/2}$. For this approximation to give a relative error in the range of few percent, it can be shown that L_{OV} has to be at least twice as large as L_0 (actually for $L_{OV} = 2L_0$ the relative error is as low as 3.6%, see Figure 4).

3. Experimental Results and Discussion

With the aim of assessing the injection length, we prepared a set of devices with different gate–electrode overlaps L_{OV}, and with different channel lengths L, both varying from 5 to 40 µm (Figure 2a). Unless otherwise stated, irrespective of device dimensions we applied V_{DS} = 8 V. The samples were fabricated with lithographically defined gold source and drain contacts. P(NDI2OD-T2) was spin-coated yielding 40–50 nm thick films. We adopted a double layer dielectric stack, comprised of a 350 nm thick poly (methyl methacrylate) (PMMA) film and of a 400 nm thick alumina layer deposited by pulsed laser deposition (PLD),[41] since alumina is very effective in suppressing gate leakage currents without compromising the overall gate capacitance thanks to its high dielectric constant. The leakage current was as low as 1 nA cm^{-2} (Figure 2b).

We fabricated devices with intrinsic (net of contact resistances effect) mobility in the range of 0.1 cm^2 V^{-1} s^{-1}, in agreement with previous reports for analogously processed P(NDI2OD-T2)-based OTFT.[24,42]

3.1. Extraction of OTFT Parameters from Experimental Data

The quantity L_0 and therefore the ordering relation between L_0 and L_{OV} are a priori unknown. Therefore experimental data is tentatively analyzed using both the approximations reported in Sections 2.2.1. and 2.2.2, verifying a posteriori which one applies.

If $L_{OV} \leq L_0$ the functional form of contact resistances introduced in Section 2.2.1. (Equation (4)), allows the extraction of OTFT parameters by means of the Differential Method (DM),[23] which advantageously exploits integral and differential operators to progressively reduce the number of unknowns. The range for parameter extraction is V_G = 70–80 V, where we find that the assumptions of DM are verified.[23] For each single device we extract R_{CTOT}, γ, V_T, and μ_0.

If $L_{OV} \geq 2L_0$ the DM cannot be applied (contact resistances depending on $(V_G - V_T)^{-(\gamma+1)/2}$ are not dealt with), hence we resort to non-linear fitting of the transfer characteristic curves (see Supporting Information). The fitting range is the same used in the DM (V_G = 70–80 V).

Contact resistances are plotted in **Figure 5**a: their order of magnitude is tens of kΩcm. With the chosen bias of V_{DS} = 8 V, the inequality $L_{OV} \leq L_0$ is met in the following cases: L = 20 µm, L_{OV} = 5 µm; L = 40 µm with L_{OV} = 5 and 10 µm.

The relative weight of contact resistances, shown in Figure 5b, is not negligible: it is as large as 20% of the total device resistance for L = 20 µm and for L = 40 µm, and about 40% for L = 5 µm. Note that $R_{C\,REL}$ is mainly determined by the ratio L/L_0, because in most of the cases the ratio L_{OV}/L_0 is large enough to make the term $\tanh(L_{OV}/L_0)$ in Equation (2) very close to 1 (see Figure S4 in the Supporting Information). Injection lengths are reported in **Table 1**.

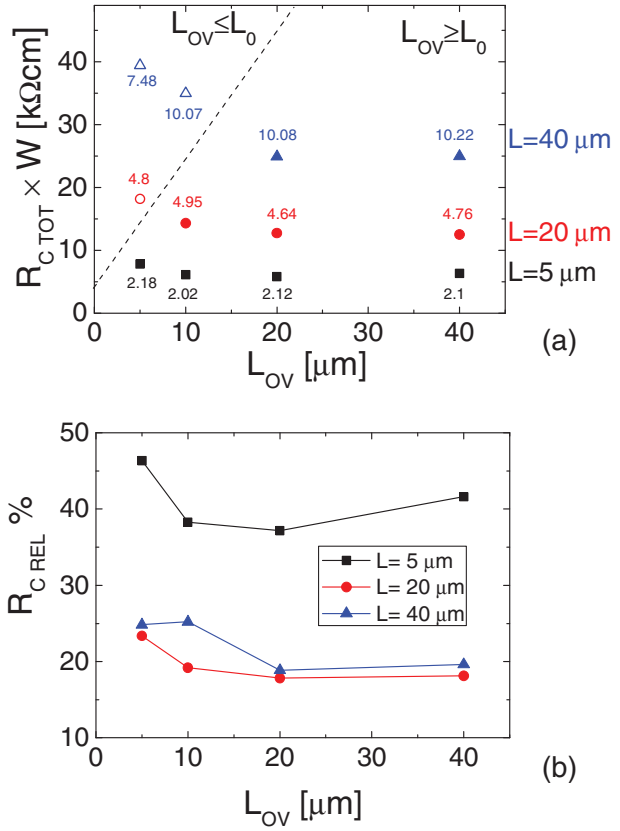

Figure 5. Panel a) shows extracted width normalized contact resistance R_{CTOT} versus overlap length L_{OV} measured at V_{DS} = 8 V. Hollow (solid) symbols indicate that $L_{OV} \leq L_0$ ($L_{OV} \geq 2L_0$); the numerical label up or below the symbols is the value of L_0 (unit of measure micrometers). Panel b) shows the relative weight of contact resistances R_{CREL}%. In both panels channel lengths L = 5, 20, 40 μm are reported in black squares, red circles, and blue triangles, respectively.

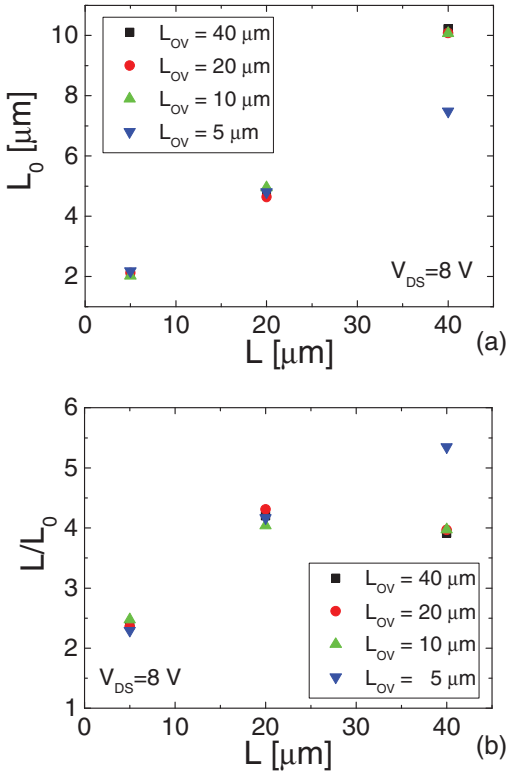

Figure 6. Panel a) shows the injection length L_0 versus the channel length. Panel b) shows the ratio L/L_0 versus channel length. V_{DS} = 8 V.

3.2. Analysis of Results

In agreement with the theory outlined in Section 2. for a fixed L, R_{CTOT} is a decreasing function of L_{OV} and tends to a constant value for large L_{OV} (Figure 5a). Unexpectedly, $R_{C\,TOT}$ depends on L as well: the shorter is L, the smaller is R_{CTOT}. This occurs because L_0 depends on L in its turn (Table 1, **Figure 6**a): it is equal to about 10 μm for L = 40 μm about 5 μm for L = 20 μm and about 2 μm for L = 5 μm. This is somewhat surprising because one would expect L_0 to be independent of device physical dimensions being a function of R_γ and R_{sh}. Before investigating the physical origins of this finding, we focus on its consequences: on shortening the channel length *at fixed bias voltage*, the increase of the relative weight of contact resistances is milder than expected. In fact, going from L = 40 μm down to L = 20 μm R_{CREL} is not sizeably affected (see Figure 5b), thanks to the fact the ratio L/L_0 is practically constant as shown in Figure 6b (with the exception of the device having L = 40 μm and L_{OV} = 5 μm). Further scaling L down to 5 μm results in a deterioration of R_{CREL} which reaches about 40%, due to the fact that the dependence of L_0 on L is milder than on longer channels. Yet, if L_0 were constant (and equal to 10 μm as it is found for L = 40 μm), R_{CREL} would be as high as 70%–80% for L = 5 μm (Figure S5, Supporting Information).

Table 1. OTFTs experimental injection lengths (V_{DS} = 8 V).

L_{OV} [μm]	L_0 [μm]	L_0 [μm]	L_0 [μm]
	L = 5 μm	L = 20 μm	L = 40 μm
5	2.18	4.8	7.48
10	2.02	4.95	10.7
20	2.12	4.64	10.08
40	2.1	4.76	10.22

The origin of the dependence of L_0 on L has to be traced back to the fact that R_{C_γ} is a function of the drain–source applied voltage (R_{sh} is substantially constant, see Figure S6 in the Supporting Information). In **Figure 7** we plot J versus $\Delta V_{R_{CTOT_\gamma}}$, where J is the contact current density and $\Delta V_{R_{CTOT_\gamma}}$ is the voltage drop on $R_{C\,TOT_\gamma}$ (equal to the current multiplied by $R_{C\,TOT_\gamma}$) for various V_{DS}. Upon increasing V_{DS}, the voltage drop $\Delta V_{RC\,TOT_\gamma}$ increases as well, but the various J segments do not belong to the same line: the inverse slope of the segments, that is $R_{CTOT\gamma}$, is a decreasing function of $\Delta V_{RC\,TOT_\gamma}$. This is in agreement with previous studies on P(NDI2OD-T2)-based OTFTs with Au contacts,[38] where it was demonstrated that injection—which dominates over transport across γ-axis thanks to the high bulk mobility of P(NDI2OD-T2)—is a highly non-linear

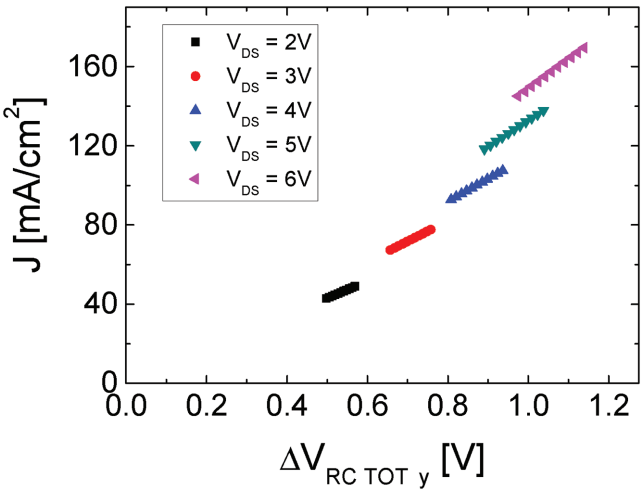

Figure 7. Plot of J versus $\Delta V_{R_{C\,TOT_y}}$: $L = 20$ µm, $L_{OV} = 5$ µm, and V_{DS} varies from 2 to 6 V. For a fixed V_{DS}, $\Delta V_{R_{C\,TOT_y}}$ was extracted by means of DM (since $L_{OV} \leq L_0$) by varying V_G from 70 to 80 V.

phenomenon because the reverse-biased source/semiconductor junction is subject to the Schottky barrier-lowering effect. When L is down-scaled while keeping V_{DS} constant, the channel resistance gets smaller, the voltage drop across $R_{C\,TOT_y}$ gets larger and carrier injection is super-linearly enhanced.

4. Conclusions

In the framework of staggered OTFTs with contacts operating in the current crowding regime, we have introduced the relative weight of contact resistance with respect to overall device resistance, viz. R_{CREL}, as a figure of merit to quantify the degree of limitation introduced by injection issues. R_{CREL} is a function of two ratios: the channel length over the injection length, viz. L/L_0, and the overlap length over the injection length, viz. L_{OV}/L_0. If this latter is made sufficiently large (at least 1.5) so that injection is not limited by the overlap length, the value of R_{CREL} is practically set by the former ratio. We introduced basic design rules, viz. constraints between L and L_{OV} to be satisfied in order to ensure a certain value for R_{CREL}. We found that L/L_0 is lower bounded: for instance, $R_{CREL} = 10\%$ requires L/L_0 to be no less than 18. If in addition to a certain R_{CREL} one wants to minimize the device footprint, L and L_{OV} are unambiguously set: for instance, with $R_{CREL} = 10\%$, $(L + L_{OV})/L_0 = 20.65$. It thus turns out that the injection length is a fundamental quantity for proper transistor design because, together with the desired value for R_{CREL}, sets the device dimensions.

Then we have tackled the assessment of the injection length from experimental measurements, which requires the extraction of intrinsic carrier mobility and contact resistances. To accomplish this task easily, we have approximated the exact expression of the contact resistance—which contains a transcendental function—obtaining purely algebraic functions in two limiting cases, viz. when the overlap length is either larger or smaller than the characteristic injection length. For each case we apply an ad hoc extraction procedure according to the contact resistance functional dependence on the gate voltage: a non-linear fitting in the former case and the differential method[23] in the latter. Since the condition which applies—and hence the method to be applied—are not known a priori, the validity of the extracted parameters needs a posteriori verification.

Within this framework, we have analyzed a set of P(NDI2OD-T2)-based transistors with variable channel length and gate/contact overlap while keeping V_{DS} constant. It is known that for P(NDI2OD-T2)-based transistors metal to semiconductor carrier injection dominates over transport across the bulk and—being a non-linear phenomenon—results in a dependence of contact resistance on the drain to source voltage.[38] Here we have quantitatively investigated the impact of this phenomenon on the injection length, which turns out to depend on the channel length, going from about 10 µm for $L = 40$ µm down to about 2 µm for $L = 5$ µm. Consequently, when scaling L at constant drain to source voltage, it is possible—to a certain degree—to scale L_{OV} as well without sizeably compromising the relative weight of contact resistances. This result is not trivial because basic current crowding theory predicts the injection length to be a function of material properties but to be independent on device physical dimensions: if this were true, device downscaling would be inevitably accompanied by a large increase of the relative weight of contact resistances.

The scalability of the device footprint is expected not to be specific to P(NDI2OD-T2) because it ultimately relies on a general phenomenon: the inherent non-linearity of carrier injection due to the Schottky barrier lowering. This latter is a prominent and dominant effect in P(NDI2OD-T2) with Au contacts because: (i) the semiconductor has a sufficiently high bulk mobility so that R_y is dominated by injection; (ii) the injection barrier is relatively large, so that the relative weight of contact resistances is not negligible. For semiconductors satisfying condition (i), contacted with electrodes satisfying condition (ii) we expect our observations to be applicable. In addition we note that recent simulations predict a sizeable effect of the Schottky effect for barriers comprised between 0.3 and 0.6 eV.[36] The case of P(NDI2OD-T2) and gold contacts fits within this window, considering for the former a lowest unoccupied molecular orbital of 4.0 eV and an effective work function for the latter, which is solvent treated and ambient air contaminated, of 4.5 eV.[43]

To summarize, when dealing with a new material it is important to assess the injection length on a set of devices with different channel length. There are strong indications suggesting that non-linearity in contact resistances might be a general phenomenon in polymers with high bulk mobility and non-negligible injection barriers. An—at least partial—scalability of the gate to contacts overlap and a reasonable trade-off between transport performances and frequency behavior is within reach in the framework of organic electronics.

5. Experimental Section

Alkali-free 1737F glass slides were used as substrates which were sequentially cleaned in an ultrasonic bath with deionized water, acetone, and isopropanol, and finally by an oxygen plasma treatment for 10 min for each step. 35 nm thick Au source and drain contacts on a 1.7 nm Cr adhesion layer were patterned by a conventional photolithographic lift-off

technique. Channel lengths L and contacts lengths L_{OV} varied from 5 to 40 μm and channel width W = 1 mm. P(NDI2OD-T2 (Polyera ActivInk N2200) was dissolved in anhydrous 1,2-dicholorobenzene at 120 °C in glovebox for 40 min to obtain an 9 mg mL^{-1} solution. The solution was then filtered through a 0.2 μm PTFE filter and deposited in glovebox by spin-coating at 1000 rpm for 90 s to obtain a thickness about 40–45 nm. The samples were then annealed for 12 h at 120 °C on a hotplate. An ≈350 nm thick layer of PMMA dielectric was deposited on top of the semiconductor film by spin-coating in glove-box at 2000 rpm for 60 s from a 60 g L^{-1} *n*-butyl acetate solution of PMMA. After annealing in glovebox for 5 h at 80 °C, a ≈400 nm thick layer of aluminum oxide was deposited as a gate insulator on top of the PMMA by PLD at room temperature to suppress the gate leakage current. Finally, a 50 nm thick Al gate electrode was thermally evaporated and a post-annealing of 24 h at 120 °C in glove box was performed. It was found that long annealing time is necessary to obtain a good *I–V* characteristic curve, especially in the sub-threshold region.

Supporting Information

Supporting Information is available from the Wiley Online Library or from the author.

Acknowledgements

Fondazione Cariplo financially supported part of this work under project Indixi, Grant No. 2011-0368. M. C. acknowledges the European Research Council (ERC) for financial support through the European Union's Horizon 2020 research and innovation program "HEROIC," grant agreement 638059.

Received: March 6, 2016
Revised: June 11, 2016
Published online: July 13, 2016

[1] H. Sirringhaus, *Adv. Mater.* **2014**, *26*, 1319.
[2] Y. Gao, X. Zhang, H. Tian, J. Zhang, D. Yan, Y. Geng, F. Wang, *Adv. Mater.* **2015**, *27*, 6753.
[3] B. Nketia-Yawson, H.-S. Lee, D. Seo, Y. Yoon, W.-T. Park, K. Kwak, H. J. Son, B. Kim, Y.-Y. Noh, *Adv. Mater.* **2015**, *27*, 3045.
[4] H. H. Choi, J. Y. Baek, E. Song, B. Kang, K. Cho, S.-K. Kwon, Y.-H. Kim, *Adv. Mater.* **2015**, *27*, 3626.
[5] H.-R. Tseng, H. Phan, C. Luo, M. Wang, L. A. Perez, S. N. Patel, L. Ying, E. J. Kramer, T.-Q. Nguyen, G. C. Bazan, A. J. Heeger, *Adv. Mater.* **2014**, *26*, 2993.
[6] Y. Yamashita, F. Hinkel, T. Marszalek, W. Zajaczkowski, W. Pisula, M. Baumgarten, H. Matsui, K. Müllen, J. Takeya, *Chem. Mater.* **2016**, *28*, 420.
[7] G. Kim, S.-J. Kang, G. K. Dutta, Y.-K. Han, T. J. Shin, Y.-Y. Noh, C. Yang, *J. Am. Chem. Soc.* **2014**, *136*, 9477.
[8] J. Li, Y. Zhao, H. S. Tan, Y. Guo, C.-A. Di, G. Yu, Y. Liu, M. Lin, S. H. Lim, Y. Zhou, H. Su, B. S. Ong, *Sci. Rep.* **2012**, *2*, 754.
[9] J. Yao, C. Yu, Z. Liu, H. Luo, Y. Yang, G. Zhang, D. Zhang, *J. Am. Chem. Soc.* **2016**, *138*, 173.
[10] G. Dell'Erba, A. Luzio, D. Natali, J. Kim, D. Khim, D.-Y. Kim, Y.-Y. Noh, M. Caironi, *Appl. Phys. Lett.* **2014**, *104*, 153303.
[11] S. G. Bucella, A. Luzio, E. Gann, L. Thomsen, C. R. McNeill, G. Pace, A. Perinot, Z. Chen, A. Facchetti, M. Caironi, *Nat. Commun.* **2015**, *6*, 8394.
[12] R. Matsidik, H. Komber, A. Luzio, M. Caironi, M. Sommer, *J. Am. Chem. Soc.* **2015**, *137*, 6705.
[13] F. Ante, D. Kälblein, T. Zaki, U. Zschieschang, K. Takimiya, M. Ikeda, T. Sekitani, T. Someya, J. N. Burghartz, K. Kern, H. Klauk, *Small* **2012**, *8*, 73.
[14] T. Uemura, T. Matsumoto, K. Miyake, M. Uno, S. Ohnishi, T. Kato, M. Katayama, S. Shinamura, M. Hamada, M.-J. Kang, K. Takimiya, C. Mitsui, T. Okamoto, J. Takeya, *Adv. Mater.* **2014**, *26*, 2983.
[15] M. Uno, T. Uemura, Y. Kanaoka, Z. Chen, A. Facchetti, J. Takeya, *Org. Electron.* **2013**, *14*, 1656.
[16] Y.-Y. Noh, N. Zhao, M. Caironi, H. Sirringhaus, *Nat. Nanotechnol.* **2007**, *2*, 784.
[17] S. G. Bucella, A. Luzio, E. Gann, L. Thomsen, C. R. McNeill, G. Pace, A. Perinot, Z. Chen, A. Facchetti, M. Caironi, *Nat. Commun.* **2015**, *6*, 8394.
[18] M. Kitamura, Y. Arakawa, *Jpn. J. Appl. Phys.* **2011**, *50*, 01BC01.
[19] M. Kitamura, Y. Arakawa, *Appl. Phys. Lett.* **2009**, *95*, 023503.
[20] T. Zaki, R. Rödel, F. Letzkus, H. Richter, U. Zschieschang, H. Klauk, J. N. Burghartz, *Org. Electron.* **2013**, *14*, 1318.
[21] M. Uno, B.-S. Cha, Y. Kanaoka, J. Takeya, *Org. Electron.* **2015**, *20*, 119.
[22] K. Nakayama, M. Uno, T. Uemura, N. Namba, Y. Kanaoka, T. Kato, M. Katayama, C. Mitsui, T. Okamoto, J. Takeya, *Adv. Mater. Interfaces* **2014**, *1*, 1300124.
[23] D. Natali, L. Fumagalli, M. Sampietro, *J. Appl. Phys.* **2007**, *101*, 014501.
[24] D. Natali, M. Caironi, *Adv. Mater.* **2012**, *24*, 1357.
[25] A. Risteska, K. Myny, S. Steudel, M. Nakamura, D. Knipp, *Org. Electron.* **2014**, *15*, 461.
[26] H. Klauk, G. Schmid, W. Radlik, W. Weber, L. Zhou, C. D. Sheraw, J. a. Nichols, T. N. Jackson, *Solid State Electron.* **2003**, *47*, 297.
[27] E. Ehrenfreund, C. Lungenschmied, G. Dennler, H. Neugebauer, N. S. Sariciftci, *Appl. Phys. Lett.*, **2007**, *91*, 012112.
[28] C.-H. Shim, F. Maruoka, R. Hattori, *IEEE Trans. Electron Devices* **2010**, *57*, 195.
[29] M. Caironi, Y.-Y. Noh, H. Sirringhaus, *Semicond. Sci. Technol.* **2011**, *26*, 034006.
[30] K. Jung, Y. Kim, B. Park, H. Shin, J. Lee, *IEEE Trans. Electron Devices* **2009**, *56*, 431.
[31] T. J. Richards, H. Sirringhaus, *J. Appl. Phys.* **2007**, *102*, 094510.
[32] A. Benor, D. Knipp, *Org. Electron.* **2008**, *9*, 209.
[33] Y. Xu, C. Liu, W. Scheideler, P. Darmawan, S. Li, F. Balestra, G. Ghibaudo, K. Tsukagoshi, *Org. Electron.* **2013**, *14*, 1797.
[34] J. Park, L.-M. Do, C. Pearson, M. Petty, D. W. Kim, J. S. Choi, *Jpn. J. Appl. Phys.* **2012**, *51*, 09MJ01.
[35] H. Wang, W. Wang, P. Sun, X. Ma, L. Li, M. Liu, Y. Hao, *IEEE Electron Device Lett.* **2015**, *36*, 609.
[36] M. Gruber, F. Schürrer, K. Zojer, *Org. Electron.* **2012**, *13*, 1887.
[37] A. Luzio, L. Criante, V. D'Innocenzo, M. Caironi, *Sci. Rep.* **2013**, *3*, 3425.
[38] M. Caironi, C. Newman, J. R. Moore, D. Natali, H. Yan, a. Facchetti, H. Sirringhaus, *Appl. Phys. Lett.* **2010**, *96*, 183303.
[39] K.-D. Jung, Y. C. Kim, B.-J. Kim, B.-G. Park, H. Shin, J. D. Lee, *Jpn. J. Appl. Phys.* **2008**, *47*, 3174.
[40] M. Vissenberg, M. Matters, *Phys. Rev. B* **1998**, *57*, 964.
[41] A. Luzio, F. G. Ferré, F. Di Fonzo, M. Caironi, *Adv. Funct. Mater.* **2013**, *24*, 1790.
[42] H. Yan, Z. Chen, Y. Zheng, C. Newman, J. R. Quinn, F. Dötz, M. Kastler, A. Facchetti, *Nature* **2009**, *457*, 679.
[43] S. Braun, W. R. Salaneck, M. Fahlman, *Adv. Mater.* **2009**, *21*, 1450.

